INTERNATIONAL JOURNAL OF AUTOMOTIVE AND MECHANICAL ENGINEERING
ISSN: 2229-8649 e-ISSN: 2180-1606
VOL. 20, ISSUE 4, 2023, 10838 – 10849
DOI: https://doi.org/10.15282/ijame.20.4.2023.03.0838

RESEARCH ARTICLE

Numerical Study on the Torsional and Lateral Vibrations of Double Universal Joint Driveline System

M. H. Omar[1,*], M. A. Rahim[2], M. N. A. M. Rejab[1]

[1]Faculty of Mechanical Engineering and Technology, Universiti Malaysia Perlis, 02600 Arau, Perlis, Malaysia
[2]Faculty of Electrical Engineering and Technology, Universiti Malaysia Perlis, 02600 Arau, Perlis, Malaysia

ABSTRACT - Utilizing a universal joint can lead to significant vibration within a driveline system. This study presents a model for analyzing the torsional and lateral vibrations of a driveline connected by a double universal joint. The governing equations of motion are derived, and the Runge-Kutta method computes steady-state responses across a spectrum of input rotational speeds. The focus is to examine the effect of system parameters, including static angular misalignment, load torque, and lateral stiffness. Relative amplification is used to analyze the effects of parameters on system vibration. Results indicated that the second-order component of input rotational speed induced by the universal joint was the factor that caused the vibrations. For the considered system, static angular misalignment significantly impacts both the torsional and lateral vibrations. Increasing the angular misalignment from 15° to 30° results in a threefold increase in lateral vibration amplification, while torsional vibration amplification is increased by nearly two times. The effect of load torque is almost linearly proportional to torsional vibration but is nonlinear to lateral vibration. Thus, lateral vibration is significantly impacted compared to torsional vibration for higher load torque. Changing the stiffness leads to a modification of the natural frequency. Increasing the lateral stiffness shifts the critical speed to a higher speed range, resulting in reduced lateral vibration amplitude. It is demonstrated that a slight fluctuation in angular misalignment due to lateral vibration will not affect the torsional vibration even if both vibrations are coupled. The findings may enhance understanding of how changing system parameters affects vibration.

ARTICLE HISTORY
Received : 23rd May 2023
Revised : 24th Aug. 2023
Accepted : 25th Oct. 2023
Published : 26th Dec. 2023

KEYWORDS
Universal joint
Driveline system
Torsional and lateral vibrations
Second-order vibration

1.0 INTRODUCTION

The driveline system is a prominent source of noise and vibration in vehicles, spanning from cars to high-speed trains [1–3]. The vibrational properties of drivelines are currently an essential practical issue due to their potential to cause boom noise and gear rattle, which can negatively impact vehicle performance and passenger comfort [4–6]. The automotive driveline system includes various components, including the transmission, drive shafts, universal joints, and main reducer. The propeller shaft and universal joints are a significant source of driveline system vibration among the components. A Cardan or universal joint is a mechanical coupling between two misaligned rotating shafts. It is used in various systems, such as automobiles, agricultural, and rail vehicles [7]. When there is an angular misalignment, the driveline connected by a universal joint can experience fluctuations in the driven shaft speed and the lateral moment [8]. The fluctuations can cause undesirable vibrations in torsional and lateral directions. These vibrations can excite the system's natural frequencies and lead to instability under certain conditions.

Several attempts have been made to investigate vibration problems in specific components of a vehicle driveline system through the Multi-Body System (MBS) method. The aim is to derive valuable kinematic and dynamic information from simulations to replace a portion of the testing procedure and minimize testing expenses. Liu et al. [9] developed a hybrid approach that combines MBS and Finite Element Analysis (FEA) to precisely predict the occurrence of high-frequency driveshaft moan vibration caused by universal joints. The proposed approach was validated by comparing it with test rig and vehicle test data to analyze the second-order and fourth-order vibrations caused by the universal joint. Qiu and Shangguan [10] developed a kinematic model for the double roller tripod joint to analyze its kinematic characteristics and provide a theoretical foundation for its application and enhancement. The kinematic model of the double roller tripod universal joint was verified through motion simulation in ADAMS software. In their study, Yu et al.[11] employed the MBS method to predict the torque transmission efficiency of constant velocity joints (CVJ). Next, an analysis was conducted to examine the theoretical foundation behind the high transmission efficiency of the high-efficiency joint, specifically focusing on contact force and friction. Li et al. [12] developed a methodology for calculating and analyzing the secondary torque caused by the ball-type universal joint using the MBS approach. The model examines the impact of various parameters on the secondary torque.

Interaction between the two vibration modes, or one vibration inducing an oscillation in the other coupled mode, may cause undesirable vibration in the rotor system. There have long been issues with coupled vibration in a rotating system. Engineers have frequently been concerned by their existence and frequency response characteristics. Han et al. [13, 14]

***CORRESPONDING AUTHOR | M. H. Omar** | ✉ hazriomar@hotmail.com

showed that the coupled torsional and lateral vibration causes high torsional vibration in the propulsion shaft system of a ship. The impact of a significant rotor imbalance resulting from a fan blade breakage during gas turbine engine operation on the combined torsional and lateral vibration was investigated by Hong et al. [15]. The study extensively addresses the correlation between the modes and responses exhibited by an unbalanced rotor. Shen and Lu [16] developed a model of coupled torsional-lateral-longitude vibration of vehicular drivelines to study the interior boom problems. Wahab et al. [17] investigated the effect of torsional deformation on the dynamic instability of a high-speed rotating Timoshenko shaft system. A parametric instability chart was calculated with Bolotin's method to study the shaft system with different boundary conditions.

Many studies have been conducted on the coupled torsional and lateral dynamics of driveline systems driven by a single universal joint. The instability of lateral and torsional vibrations was observed by Kato et al. [18, 19]. They found that the combination of two natural frequencies about bending and torsional, when nearly coinciding with the twice input rotational speed, led to the instability of stated vibrations. The region of instability exhibited an upward trend in response to an increase in angular misalignment. At the same time, it demonstrated a downward trend in response to an increase in the viscous damping coefficient of torsional vibration as opposed to bending vibration. DeSmidt et al. [20] conducted a study investigating the dynamics of a rotor disc system connected to soft support and propelled through a universal joint. The Floquet theory was employed to examine the stability of the system across varying degrees of angular misalignment. The results of the study indicated that angular misalignment could result in dynamic coupling, which may cause parametric instability near the sum-type combinations of lateral and torsional natural frequencies. Xia et al. [21, 22] conducted a numerical study considering the additional bending moment caused by the universal joint. The torsional and lateral vibrations were excited by the second-order component of input rotational speed. However, the sum-type combination of the natural frequencies is not observed. The numerical results were verified using the experimental study on the 4WD vehicle. Tchomeni et al. [23, 24] investigated the dynamic characteristics of two misaligned rotors under the influence of an unbalanced rotor. The vibration caused by misalignment and unbalance has a second-order frequency component.

Regarding the dynamic of double universal joint driveline systems, Browne and Palazzolo [25] developed an analytical model of a secondary moment to study the nonlinear lateral vibration caused by the universal joint. Results showed that the secondary moment is proportional to the angular misalignment and the load inertia. Compared to load inertia, the variations in angular misalignment significantly impact the lateral vibration. Using the monodromy matrix, SoltanRezaee et al. [26, 27] investigated the torsional stability of three flexible shafts under the effects of angular misalignment, damping, and stiffness values. Several zones of resonance have been discovered, with the parametric resonances associated with lower natural frequencies being the most clearly recognized. Bharti and Samantaray [28] examined the Sommerfeld effect caused by torsional vibration in the driveline system configured in large angular misalignment. Two regions of resonance capture and escape phenomenon were observed, one near half of the natural frequency and the other at that natural frequency. When a constantly high torque is applied, the Sommerfeld effect is always visible when the speed range is half the natural frequency. However, there is no symptom of the Sommerfeld effect as the speed range approaches the natural frequency. Reducing angular misalignments or boosting shaft torsional damping could help to lower vibration amplitude and avoid Sommerfeld effects. The Sommerfeld effect resulting from the coupling of torsional and lateral vibrations of the driveline was assessed by Yao and DeSmidt [29]. Investigations were conducted to analyze the vibrations under varying conditions of static angular misalignment and lateral damping values. The observation of the Sommerfeld effect was limited to a speed range that corresponded to half of the torsional natural frequency. Hence, it was concluded that the phenomenon of speed capture is mainly attributed to the torsional mode.

A driveline connected by a pair of universal joints suffers torsional and lateral vibrations due to the kinematics of the universal joints. These vibrations might lead to the failure of the shaft and other components. Previous studies have not thoroughly examined a comprehensive model of this particular system. The reason for this separation in the study of vibrations is due to the distinct nature of these two types of vibrations. Additionally, previous research has predominantly focused on systems that incorporate a single universal joint. This study presents a model for analyzing the torsional and lateral vibrations of a driveline connected by a double universal joint to predict these vibrations in their design state. Analyzing the vibration of the system using mathematical models and simulations can help identify potential issues and design solutions. The governing equations representing the dynamics of the system are derived using the Lagrange method. The developed model integrates the torsional damping effect and the complete kinematics relationship of the universal joint into the equation of lateral vibration. The Runge-Kutta method computes steady-state responses of the angle of twist and dynamic angular misalignment across a spectrum of input rotational speeds. A relative amplification value is employed to examine the impacts of static angular misalignment, load torque, and lateral stiffness on the system vibration.

2.0 METHODOLOGY

The methodology for the current investigation is structured as follows. The study commenced by developing a dynamic model of the driveline system. The system description section provides further information on the system's parameters and underlying assumptions. The equations of motion are then derived using Lagrange's equations. The numerical method subsection focuses on establishing a theoretical foundation for numerical simulation. Its purpose is to

determine both the steady-state twist and dynamic angular misalignment. The effects of system parameters, including static angular misalignment, load torque, and lateral stiffness, on the torsional and lateral vibrations are discussed in the result and discussion section. Figure 1 summarizes the process involved in this study.

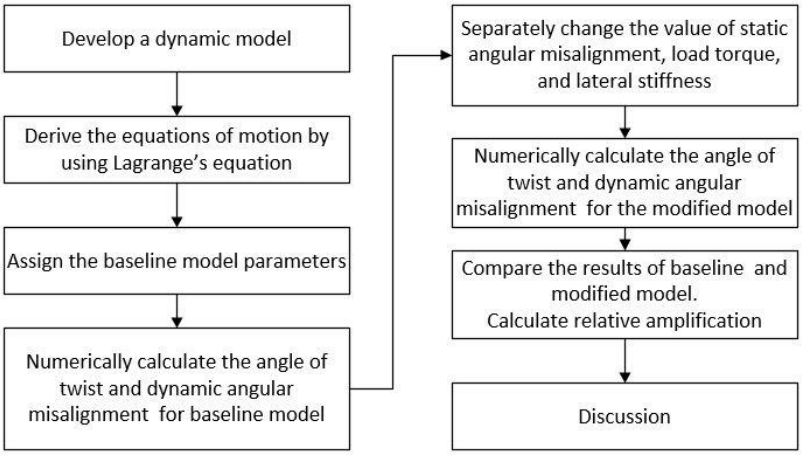

Figure 1. Flowchart of methodology

2.1 System Description

The diagram presented in Figure 2 illustrates a schematic representation of the driveline system incorporating a double universal joint. The system configuration comprises three shafts interconnected by two sets of universal joints, wherein the drive and driven shafts exhibit rigidity. The intermediate shaft has a length denoted by L_c and possesses an external diameter of d_o. It is assumed that the intermediate shaft with torsional stiffness, k_θ and torsional damping, c_θ is attached to the input and output shafts with an equal static angular misalignment, β. The present system is susceptible to angular misalignment solely in the XZ plane. The suspended mass, m_s is supported by a support structure with translational stiffness, k_ϕ, and translational damping, c_ϕ, which act on the Z-axis. The driven side is characterized by a lumped moment of inertia denoted as J_{load} and is subjected to an axial load torque, T_{load}. In modeling the system, a few assumptions are made. First, the stiffness of the support structure is considered to be lower than that of the output shaft's bending stiffness. As a result, according to Yao and DeSmidt [29], the suspended mass undergoes rigid lateral modes along the Z-axis, with both universal joints remaining in equal angular misalignment. Second, the intermediate shaft is massless as its contributions to inertia are typically much smaller than those of J_{load} and m_s. Third, the intermediate shaft's natural frequencies for the bending mode are significantly higher than those for the torsional modes. For the damping effect in the system, it is represented by $c_\theta = \xi_\theta c_\theta$, and $c_\phi = \xi_\phi c_\phi$, where ξ_θ and ξ_ϕ denote the viscous damping coefficient. The driveline runs under a constant input rotational speed, where the angular position of the input shaft and output shaft are labeled as φ_1 and φ_4, respectively. Meanwhile, the angular position of the intermediate shaft on the drive side is denoted as φ_2, and on the driven side is denoted as φ_3. The calculation of dynamic angular misalignment resulting from the elastic deformation of the support is performed by applying the moment equation around point 1. Table 1 provides the parameter values selected for the current investigation.

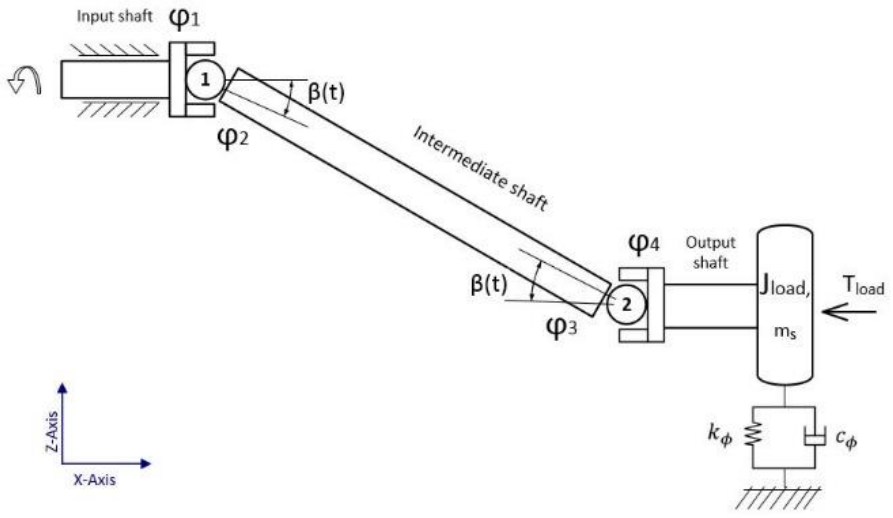

Figure 1. Double universal joint driveline dynamic model schematic

Table 1. Model parameters of the double universal joint driveline system

Description	Symbol	Value	Unit
Outer diameter of the intermediate shaft	d_o	0.010	m
Length of the intermediate shaft	L_c	0.325	m
Moment of inertia of the driven side	J_{load}	0.0045	kg.m^2
Suspended mass	m_s	4.09	kg
Torsional stiffness of the intermediate shaft	k_θ	92.20	Nm.rad^{-1}
Damping coefficient of the intermediate shaft	ξ_θ	0.002	s
Load torque	T_{load}	5	Nm
Stiffness of support structures	k_ϕ	26331	N.m^{-1}
Damping coefficient of support structures	ξ_ϕ	0.002	s

2.2 Equations of Motion

The present study analyzes a two-degree-of-freedom system that represents torsional and lateral vibrations. The phenomenon of torsional vibration is depicted by an angle of twist resulting from the angular deformation occurring in the intermediate shaft, as illustrated in Figure 2. Therefore, an angle of twist and its derivative can be expressed as [30]

$$\theta_s = \varphi_3 - \varphi_2 \tag{1}$$

$$\dot{\theta}_s = \dot{\varphi}_3 - \dot{\varphi}_2 \tag{2}$$

Figure 2. The angle of twist

Initially, the intermediate shaft is connected to drive and driven shafts with static angular misalignment, β_0. Due to the bending moment generated by the universal joint, the suspended mass will experience lateral oscillations along the Z-axis. This results in the introduction of a dynamic angular misalignment, denoted as ϕ. The resulting angular misalignment, β, is hence a combination of static and dynamic angular misalignments, written as [22]

$$\beta = \beta_0 + \phi \tag{3}$$

The model of the system is created based on the kinematic equations of a single universal joint with constant angular misalignment, as illustrated in Figure 3. The kinematic correlation between the angular positions of the driving and driven yokes of a universal joint can be mathematically represented as [31]

$$tan(\varphi_2) = \frac{tan(\varphi_1)}{cos(\beta)} \tag{4}$$

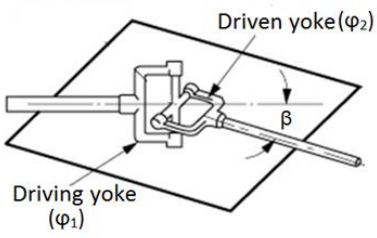

Figure 3. Single universal joint

The angular positions of the yokes on the driving and driven sides of the intermediate shaft with dynamic angular misalignments can be expressed using the kinematic relationships given in Equation 4 as

$$tan(\varphi_2) = \frac{tan(\varphi_1)}{cos(\beta_o + \phi)} \tag{5}$$

$$tan(\varphi_3) = \frac{tan(\varphi_4)}{cos(\beta_o + \phi)} \tag{6}$$

The first derivative of Equation 5 and Equation 6 gives the relationship between the angular speeds of the intermediate shaft's yokes as [32]

$$\dot{\varphi}_2 = \Omega_0 \frac{cos(\beta_o + \phi)}{1 - sin^2(\beta_o + \phi)\, cos^2(\varphi_1)} + \dot{\phi} \frac{0.5\ sin(2\varphi_1 t)\ (sin(\beta_o + \phi))}{1 - sin^2(\beta_o + \phi)\, cos^2(2\varphi_1)} \tag{7}$$

$$\dot{\varphi}_3 = \dot{\varphi}_4 \frac{cos(\beta_o + \phi)}{1 - sin^2(\beta_o + \phi)\, cos^2(\varphi_4)} + \dot{\phi} \frac{0.5\ sin(2\dot{\varphi_{out}})\ (sin(\beta_o + \phi))}{1 - sin^2(\beta_o + \phi)\, cos^2(\varphi_4)} \tag{8}$$

The current framework involves the derivation of equations of motion through the utilization of Lagrange's equations, written as

$$\frac{d}{dt}\left(\frac{\partial K}{\partial \dot{q}_i}\right) - \frac{\partial K}{\partial q_i} + \frac{\partial D}{\partial \dot{q}_i} + \frac{\partial P}{\partial q_i} = Q_i, i = 1,2,.,n \tag{9}$$

The generalized coordinate of the system is described by

$$q = \{\varphi_4 \quad \phi\}^T \tag{10}$$

The total kinetic energy of the system is expressed as

$$K = \frac{1}{2} J_{load} \dot{\varphi_4}^2 + \frac{1}{2} m_s \left(L_c\ cos\, \beta_0\, \dot{\phi}\right)^2 \tag{11}$$

The total damping dissipated energy of the system is expressed as

$$D = \frac{1}{2} c_\theta (\dot{\varphi}_3 - \dot{\varphi}_2)^2 + \frac{1}{2} c_\phi \left(L_c \cos \beta_0\, \dot{\phi}\right)^2 \tag{12}$$

$$\begin{aligned} D = \frac{1}{2} c_\theta \Bigg[& \left(\dot{\varphi}_4 \frac{cos(\beta_o + \phi)}{1 - sin^2(\beta_o + \phi)\, cos^2(\varphi_4)} + \dot{\phi} \frac{0.5\ sin(2\varphi_4)\ (sin(\beta_o + \phi))}{1 - sin^2(\beta_o + \phi)\, cos^2(\varphi_4)} \right) \\ & - \left(\dot{\varphi}_1 \frac{cos(\beta_o + \phi)}{1 - sin^2(\beta_o + \phi)\, cos^2(\varphi_1)} + \dot{\phi} \frac{0.5\ sin(2\varphi_1 t)\ (sin(\beta_o + \phi))}{1 - sin^2(\beta_o + \phi)\, cos^2(2\varphi_1)} \right) \Bigg]^2 \\ & + \frac{1}{2} c_\phi \left(L_c \cos \beta_0\, \dot{\phi}\right)^2 \end{aligned} \tag{13}$$

The total potential energy of the system is expressed as

$$P = \frac{1}{2} k_\theta (\varphi_3 - \varphi_2)^2 + \frac{1}{2} k_\phi (L_c \cos \beta_0\, \phi)^2 \tag{14}$$

$$P = \frac{1}{2} k_\theta \left(tan^{-1}\left(\frac{tan(\varphi_4)}{cos(\beta_o + \phi)}\right) - tan^{-1}\left(\frac{tan(\varphi_1 t)}{cos(\beta_o + \phi)}\right) \right)^2 + \frac{1}{2} k_\phi (L_c \cos \beta_0\, \phi)^2 \tag{15}$$

Subsequently, the equations of motion can be derived by substituting the preceding equations for the kinetic, potential, and damping dissipated energy terms into Equation 9 [22]

$$J_{load} \ddot{\varphi}_4 + c_\theta \eta_2 (\eta_2 \dot{\varphi}_4 - \eta_1 \dot{\varphi}_1) + k_\theta \eta_2 (\varphi_3 - \varphi_2) = T_{load} - c_\theta \eta_2 \dot{\phi} (\eta_{2A} - \eta_{1A}) \tag{16}$$

$$\begin{aligned} m_s (L_c \cos \beta_0)^2 \ddot{\phi} + c_\phi (L_c \cos \beta_0)^2 \dot{\phi} + \left[k_\phi (L_c \cos \beta_0)^2 \phi\right] + c_\theta \dot{\phi} (\eta_{2A} - \eta_{1A})^2 \\ = -c_\theta (\eta_{2A} - \eta_{1A})(\eta_2 \dot{\varphi}_4 - \eta_1 \dot{\varphi}_1) - k_\theta (\varphi_3 - \varphi_2)(\eta_{2A} - \eta_{1A}) \end{aligned} \tag{17}$$

From Equation 7 and Equation 8, Equation 2 can be further extended as

$$\dot{\theta}_s = (\eta_2 \dot{\varphi}_4 - \eta_1 \dot{\varphi}_1) + \dot{\phi} (\eta_{2A} - \eta_{1A}) \tag{18}$$

where

$$\eta_1 = \frac{cos(\beta_o + \phi)}{1 - sin^2(\beta_o + \phi)\, cos^2(\varphi_1)}$$

$$\eta_2 = \frac{cos(\beta_o + \phi)}{1 - sin^2(\beta_o + \phi)\, cos^2(\varphi_4)}$$

$$\eta_{1A} = \frac{0.5\ sin(2\varphi_1 t)\ (sin(\beta_o + \phi))}{1 - sin^2(\beta_o + \phi)\, cos^2(2\varphi_1)}$$

$$\eta_{2A} = \frac{0.5\ sin(2\varphi_4)\ \ (sin(\beta_o + \phi))}{1 - sin^2(\beta_o + \phi)\, cos^2(\varphi_4)}$$

2.3 Numerical Method

This study uses the fourth-order adaptive Runge– Kutta algorithm (ode45) in MATLAB software to numerically simulate the steady-state vibration responses. The time step is set as 0.001s, and the error control tolerance is taken 10^{-8} to improve the numerical accuracy [22, 27]. Equations 16 through Equation 18, which pertain to the motion of the system, are transformed into a series of first-order ordinary differential equations, as denoted by Equation 19. Before simulating the steady-state responses, the natural frequencies of the system are calculated by considering the system under zero static angular misalignment. Thus, the undamped natural frequencies of the aligned driveline can be calculated as $\omega_t = \left(\frac{k_\theta}{J_{load}}\right)^{\frac{1}{2}}$ and $\omega_l = \left(\frac{k_\phi}{m_s}\right)^{\frac{1}{2}}$ [29]. Based on the selected parameter values, the lateral and torsional modes have respective natural frequencies of 143 rad/s and 80 rad/s.

$$\dot{X}_1 = X_2$$

$$\dot{X}_2 = [T_{load} - c_\theta \eta_{2\mathrm{N}} X_4(\eta_{2AN} - \eta_{1AN}) - c_\theta \eta_{2X}(\eta_{2\mathrm{N}} X_2 - \eta_{1\mathrm{N}}\dot{\varphi}_1) - k_\theta \eta_{2\mathrm{N}} X_5]/J_{load}$$

$$\dot{X}_3 = X_4$$

$$\dot{X}_4 = -\big[c_\theta(\eta_{2AN} - \eta_{1AN})(\eta_{2\mathrm{N}} X_2 - \eta_{1\mathrm{N}}\dot{\varphi}_1) - k_\theta(X_5)(\eta_{2AN} - \eta_{1AN}) - c_\phi(L_C\, cos\, \beta_0)^2 X_4 - k_\phi(L_C\, cos\, \beta_0)^2 X_3 - c_\theta X_4(\eta_{2AN} - \eta_{1AN})^2\big]/m_S(L_c\, cos\, \beta_0)^2$$

$$\dot{X}_5 = (\eta_{2\mathrm{N}} X_2 - \eta_{1\mathrm{N}}\Omega_0) + X_4(\eta_{2AN} - \eta_{1AN}) \tag{19}$$

where

$$[X_1 \quad X_2 \quad X_3 \quad X_4 \quad X_5]^T = [\varphi_4 \quad \dot{\varphi}_4 \quad \phi \quad \dot{\phi} \quad \theta_s]^T$$

$$\eta_{1\mathrm{N}} = \frac{cos(\beta_o + X_3)}{1 - sin^2(\beta_o + X_3)\, cos^2(\varphi_1)}$$

$$\eta_{2\mathrm{N}} = \frac{cos(\beta_o + X_3)}{1 - sin^2(\beta_o + X_3)\, cos^2(X_1)}$$

$$\eta_{1AN} = \frac{0.5\ sin(2\varphi_1)\ \ (sin(\beta_o + X_3))}{1 - sin^2(\beta_o + X_3)\, cos^2(2\varphi_1)}$$

$$\eta_{2AN} = \frac{0.5\ sin(2X_1)\ \ (sin(\beta_o + X_3))}{1 - sin^2(\beta_o + X_3)\, cos^2(X_1)}$$

3.0 RESULTS AND DISCUSSION

It is essential to comprehensively identify and analyze the parameters that influence the system's dynamics. The static angular misalignment is a notable parameter. In practice, most of the universal joint is designed to be operated less than 45° of angular misalignment, and their effect on driveline vibration within this range is investigated. The load torque and stiffness of the support system are additional factors that impact the system's dynamics and can be quantitatively analyzed. This section examines the impact of these parameters on the vibration of the system. The results are presented as the maximum and minimum steady-state responses observed across a range of input rotational speeds. The input rotational speed is varied within the range of 100 to 1500 rpm to encompass the system's highest natural frequency. The figures are presented as an angle of twist and dynamic angular misalignment representing the torsional and lateral vibrations, respectively.

3.1 Effect of static angular misalignment

This section examines the impact of static angular misalignment of universal joints on system vibrations based on the specified parameters listed in Table 1. Numerical simulations are carried out in the range of 15° to 30° of the static angular misalignments. Figure 4 shows the vibration responses for the static angular misalignment of 15°. The torsional vibration represented by an angle of twist in Figure 4a shows the vibration amplitude reached a peak value of 3.87° when the input rotational speed is 684 rpm. For lateral vibration shown in Figure 4b, the dynamic angular misalignment reached 0.01° when the input rotational speed was 381 rpm. By comparing with the natural frequencies of the system, the torsional and lateral vibrations are excited when twice the input rotational speed equals each of the torsional and lateral natural frequencies. This shows that the driveline system exhibits nonlinear vibration due to the kinematic relationship of the

universal joints. Mechanical systems with nonlinear characteristics can exhibit second-order vibrations. Second-order vibration is a vibration that occurs at twice the frequency of a fundamental oscillation. For the considered driveline, the primary oscillation is the input rotational speed. Therefore, the nonzero angular misalignment of the universal joint leads to the occurrence of second-order torsional and lateral vibrations. The input rotational speeds of 381 rpm and 684 are regarded as critical speeds due to the driveline experiencing significant vibrations at these speeds.

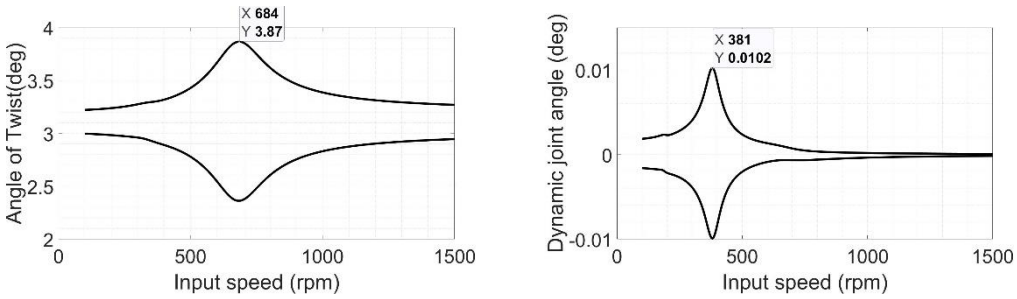

(a) Torsional vibration (b) Lateral vibration

Figure 4. Vibration responses at $\beta_o = 15°$

When the static angular misalignment is increased, the results given in Figure 5 to Figure 7 show that the largest twist amplitudes and dynamic angular misalignment are observed for static angular misalignment of 30°. This finding aligns with previous studies [20, 28] which have shown that the amplitude is proportional to the angular misalignment. Figure 7 demonstrates a minor peak at 342 rpm for torsional vibration and 190 rpm for lateral vibration in the case of a 30° static angular misalignment. These speeds correspond to the fourth-order vibration of both torsional and lateral vibrations. Previous findings [24, 33] have shown that when the angular misalignment is less than 30°, second-order vibration significantly affects vibration responses more than fourth-order vibration. Furthermore, approximating the kinematics of the universal joint relationship given in Equation 1 using the Taylor-McLaurin series up to second-order terms while ignoring the higher-order terms is feasible [27, 34]. So, the impact of fourth-order vibration on vibration responses is negligible and can be disregarded in contrast to second-order vibration. As a result, the dynamics of the system can be described by the amplitude of the second-order vibration.

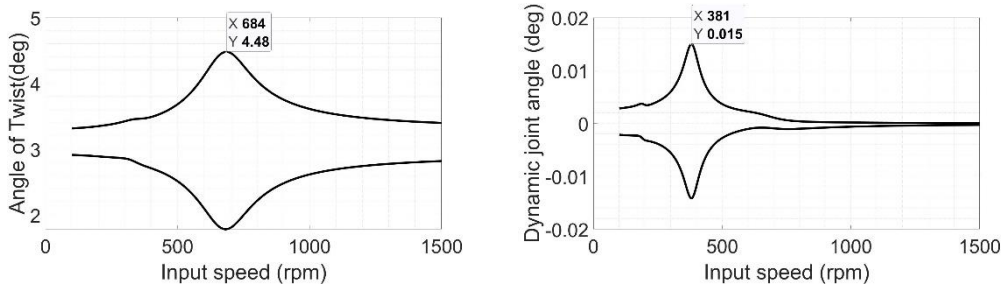

(a) Torsional vibration (b) Lateral vibration

Figure 5. Vibration responses at $\beta_o = 20°$

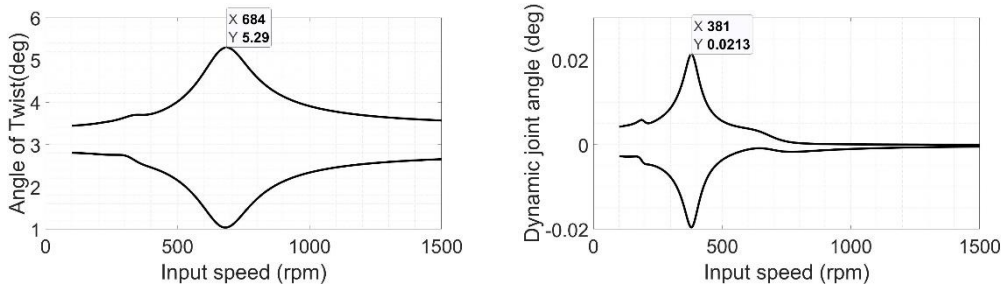

(a) Torsional vibration (b) Lateral vibration

Figure 6. Vibration responses at $\beta_o = 25°$

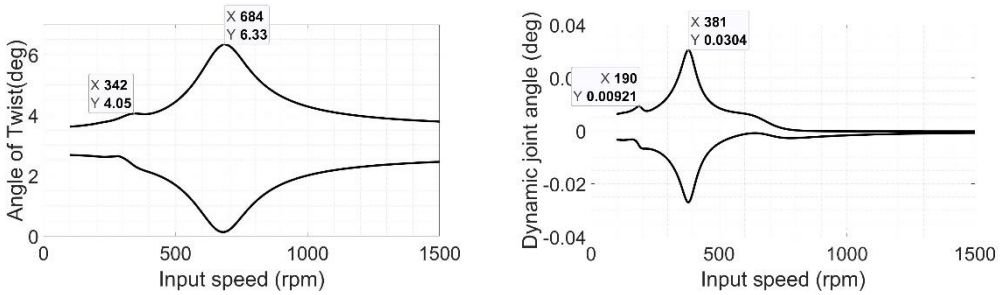

(a) Torsional vibration (b) Lateral vibration

Figure 7. Vibration responses at $\beta_o = 30°$

Relative amplification is calculated to demonstrate the effects of static angular misalignment further. Relative vibration amplification refers to the phenomenon where the amplitude or intensity of vibration is amplified due to certain conditions or factors. This amplification is measured in comparison to a reference point, often the baseline vibration level. Since the critical speeds are equal for all angular misalignments, the amplitude at these speeds due to second-order excitation is used to calculate the relative amplification. Vibration response at 15° static angular misalignment is treated as a baseline value. Figure 8 shows the calculated relative amplification for all considered values of static angular misalignments. The blue bar represents the torsional vibration, while the red bar represents the lateral vibration. The figure shows that as the static angular misalignment increases, the relative amplification increases for both vibrations. It can be seen that increasing the static angular misalignment from 15° to 30° results in a threefold increase in lateral vibration amplitude, while torsional vibration is amplified by nearly two times. Therefore, the static angular misalignment significantly impacts both the torsional and lateral vibrations.

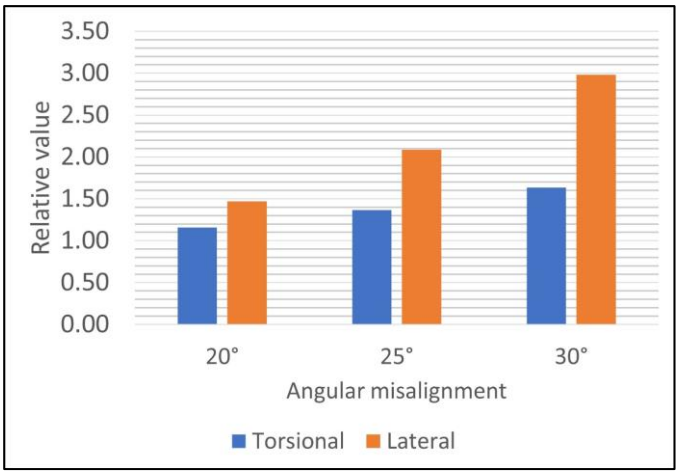

Figure 8. Relative amplification for different values of static angular misalignment

3.2 Effects of load torque

Herein, the effects of load torque on the system's dynamic will be thoroughly investigated. To display the effect, four different values of load torque, 10Nm, 15 Nm, 20 Nm, and 25 Nm, are compared with the default load torque, 5Nm. Other parameters in Table 1 are kept constant, and the static angular misalignment is fixed at 15°. When the load torque is doubled to 10 Nm, results in Figure 9 show that increasing load torque results in a higher amplitude of both torsional and lateral vibrations. However, the critical speed is in the assumed second-order vibration speed range because the natural frequencies of the system are not altered. Table 2 lists the maximum angle of twist and the maximum dynamic joint angle at critical speed for different load torque values.

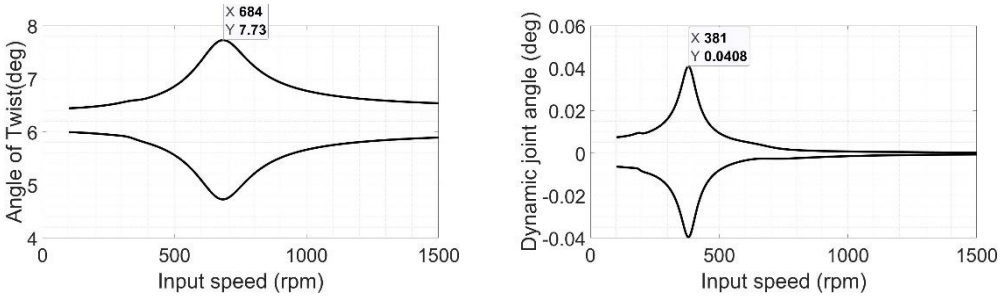

(a) Torsional vibration (b) Lateral vibration

Figure 9. Vibration responses at $T_{load} = 10Nm$

Table 2. Vibration responses at critical speed for different values of load torque

Input Torque (Nm)	Maximum angle of twist (deg)	Maximum dynamic angular misalignment (deg)
5	3.87	0.0102
10	7.73	0.0408
15	11.58	0.0915
20	15.42	0.1622
25	19.24	0.2522

The effect of the load torque on the amplification of vibration responses is shown in Figure 10. The vibration amplitude of critical speed at 5 Nm load torque is treated as a baseline value. The blue bar represents the torsional vibration, while the red bar represents the lateral vibration. The results show that the effect of load torque is almost linearly proportional to torsional vibration. For example, when the load torque is increased to 15 Nm, which is three times higher than 5 Nm, the maximum amplitude of the twist also increases three times. However, the effect of load torque on lateral vibration is in a nonlinear form. The maximum dynamic angular misalignment amplitude is amplified nine times when the input torque is increased to 15 Nm. The same finding also can be seen for 20 Nm and 30 Nm. Therefore, it is concluded that the lateral vibration is significantly affected when there are changes in load torque value.

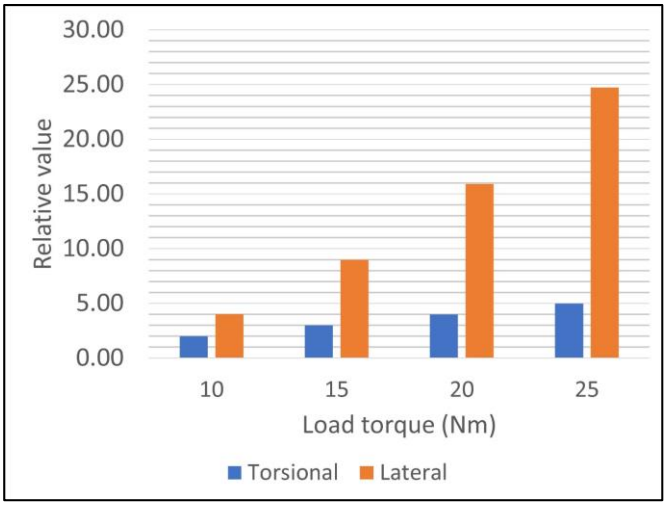

Figure 10. Relative amplification for different values of load torque

3.3 Effects of lateral stiffness

Two distinct values are considered in investigating lateral stiffness's effect on the system's dynamics. The static angular misalignment is fixed at 15° while the other parameters in Table 1 are maintained constant. The changes in the lateral stiffness result in the modification of the lateral natural frequency. In order to facilitate comparative analysis, the graph depicting the altered stiffness is graphically represented alongside the default value, as listed in Table 1. The black line represents the vibration responses of the default stiffness, 26331 Nms/rad, while the red line represents the vibration responses of the altered stiffness. For the first scenario, the lateral stiffness is reduced to 13166 Nms/rad, which is half of the default value. Reducing the lateral stiffness by 50% has modified the lateral natural frequency to 56.73 rad/s. Therefore, the critical speed due to second-order excitation has shifted to a lower speed region which is 270 rpm, as shown in Figure 11b. It is also noted that the peak amplitude has increased to 0.0287°, which means an amplification of almost three from the default value, 0.0102°. However, the torsional vibration amplitude remains unchanged, as shown in Figure 11a.

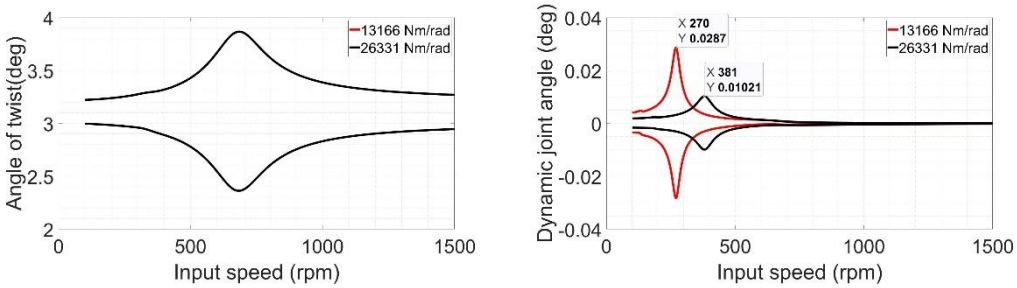

(a) Torsional vibration (b) Lateral vibration

Figure 11. Vibration responses at lateral stiffness, $k_\phi = 13166\ Nm/rad$

When the lateral stiffness is increased to 39497 Nms/rad, which is 1.5 greater than the default value, the lateral natural frequency has increased to 98.26 rad/s. The critical speed has shifted to a higher speed region, which is 468 rpm and with peak amplitude attenuated to 0.005, as shown in Figure 12b. Again, the torsional vibration amplitude remains unchanged, as shown in Figure 12a. It is essential to explain that lowering the lateral stiffness will lower the lateral natural frequency. Thus, the critical speed is shifted to a lower speed region, which may expose the driveline to higher vibration amplitude at the low speed. Increasing the lateral stiffness makes the vibration in the lateral direction safer because the critical speed is shifted to a higher speed region with a lower vibration amplitude. One observation that can be made from these two values of lateral stiffness is that minor deviations in angular misalignment are unlikely to have a significant impact on torsional vibration. This finding aligns closely with the results of Yao & DeSmidt (2021), indicating that the shaft speed capture phenomena are primarily caused by the torsional mode and not significantly affected by the driveline lateral.

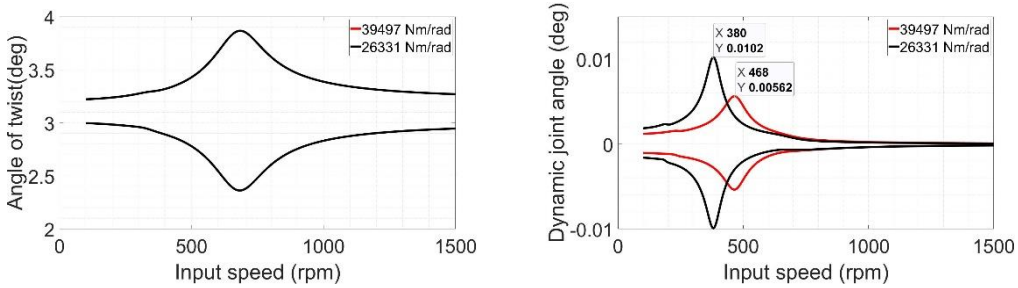

(a) Torsional vibration (b) Lateral vibration

Figure 12. Vibration responses of lateral stiffness, $k_\phi = 39497\ Nm/rad$

4.0 CONCLUSIONS

In this study, the torsional and lateral vibrations of a driveline connected by a double universal joint are studied by numerical method. The present study has devised a model that incorporates the torsional damping effect into the governing equation of lateral dynamics and the complete kinematics relationship of the universal joint. The effects of system parameters such as static angular misalignment, load torque, and lateral stiffness are discussed. The dynamic angular misalignment represents the lateral vibrations, whereas the angle of twist represents the torsional vibrations. A relative amplification is utilized to analyze the effects of these parameters on the vibration of the system. The results are summarized as follows. First, the driveline suffers second-order torsional and lateral vibrations induced by the kinematics of the universal joint. Consequently, the torsional and lateral vibrations are excited when twice the input rotational speed equals each of the torsional and lateral natural frequencies. Second, the numerical results show that the static angular misalignment significantly impacts both the torsional and lateral vibrations. When the static angular misalignment is increased, the vibration amplitudes for both vibrations are increased. So, restriction of this aspect in practical implementation is highly significant and feasible. Third, based on the relative amplification value, the impact of load torque on torsional vibration is nearly linear, while its effect on lateral vibration is nonlinear. Higher load torque has a greater impact on lateral vibration compared to torsional vibration. Fourth, lowering the lateral stiffness results in the critical speed being shifted to a lower speed range, potentially leading to increased lateral vibration amplitude in the driveline at low speeds. Enhancing the lateral stiffness shifts the critical speed to a higher speed range, reducing lateral vibration amplitude. However, a slight fluctuation in angular misalignment due to lateral vibration will not affect the torsional vibration even if both vibrations are coupled. The findings presented in this study may contribute in understanding the influence of altering system parameters on vibration, emphasizing the importance of considering these effects during design and practical applications.

5.0 REFERENCES

[1] AA. Alugongo, "Parametric vibration of a cardan shaft and sensitivity analysis," *Lecture Notes in Engineering and Computer Science*, vol. 2, pp. 691–696, 2018.

[2] J. Qu, W. Shi, J. Wang J, and Z. Chen, "Modeling and analysis of clutch nonlinear behavior in an automotive driveline for suppressing torsional vibration," *Machines*, vol. 10, no. 9, pp. 819, 2022.

[3] M. Zeng, B. Tan, F. Ding, B. Zhang, H. Zhou, and Y. Chen, "An experimental investigation of resonance sources and vibration transmission for a pure electric bus," *Proceedings of the Institution of Mechanical Engineers, Part D: Journal of Automobile Engineering*, vol. 234, pp. 950–962, 2020.

[4] Y. Hao, Z. He, G.Y. Li, E. Li, and Y. Huang, "Uncertainty analysis and optimization of automotive driveline torsional vibration with a driveline and rear axle coupled model," *Engineering Optimization*, vol. 50, no. 11, pp. 1871–1893, 2018.

[5] X. Zhang, H. Liu, Z. Zhan, Y. Wu, W. Zhang, T. Mahmoud, and P. Yan, "Modelling and active damping of engine torque ripple in a power-split hybrid electric vehicle," *Control Engineering Practice*, vol. 104, p. 104634, 2020.

[6] A.M. Al-Dhahebi, A.K. Junoh, Z. Mohamed, and W.Z.a.W. Muhamad, "A computational approach for optimizing vehicles' interior noise and vibration," *International Journal of Automotive and Mechanical Engineering*, vol. 14, no. 4, pp. 4690–4703, 2017.

[7] F. Schmelz, CH-C. Seherr-Thoss, and E. Aucktor," Universal joints and driveshafts," In *Springer eBooks*. 1992.

[8] R. Burkhalter, P.J. Mazziotti, "The low silhouette drive line," *SAE Transactions*, vol. 64, pp. 379–393, 1956.

[9] J.S. Liu, N. Remisoski, J. Iqbal, and R. Egenolf, "CAE predictions for Cardan Joint Induced Driveline NVH," *SAE Technical Paper Series*, No. 2017-01-1136, 2017.

[10] Y. Qiu, and W. Shangguan, "Kinematic analysis and simulation of the double roller Tripod joint," *SAE Technical Paper Series*, No. 2019-01-1526, 2019.

[11] X. Yu, Q. Hou, R. Zhen, and W. Shangguan, "Transmission efficiency analysis of high-efficiency constant velocity joint," *SAE Technical Paper Series*, No. 2021-01-0705, 2021.

[12] S. Li, X. Wang, R. Zhen, and R. Li, "Analysis of influencing Factors of Secondary torque of Automotive Ball-Type Universal Joint," *SAE Technical Paper Series*, No. 2021-01-0677, 2021.

[13] H.S. Han, and K.H. Lee, "Experimental verification for lateral-torsional coupled vibration of the propulsion shaft system in a ship," *Engineering Failure Analysis*, vol. 104, pp. 758–771, 2019.

[14] H. Han, K. Lee, S.H. Jeon, S.H. Park, "Lateral-torsional coupled vibration of a propulsion shaft with a diesel engine supported by a resilient mount," *Journal of Mechanical Science and Technology*, vol. 31, pp. 3727–3735 (2017)

[15] J. Hong, P. Yu, Y. Ma, and D. Zhang, "Investigation on nonlinear lateral-torsional coupled vibration of a rotor system with substantial unbalance," *Chinese Journal of Aeronautics*, vol. 33, no. 6, pp. 1642–1660, 2020.

[16] C. Shen, and C. Lu, "A refined torsional-lateral-longitude coupled vehicular driveline model for driveline boom problems," *Applied Mathematical Modelling*, vol. 90, pp. 1009–1034, 2021.

[17] A. M. A. Wahab, Z. Yusof, Z. A. Rasid, A. Abu, and N. F. M. N. Rudin, "Dynamic Instability of High-Speed Rotating Shaft with Torsional Effect," *International Journal of Automotive and Mechanical Engineering*, vol. 15, no. 4, pp. 6034–6051, Dec. 2018.

[18] M. Kato, H. Ota, and R. Kato, "Lateral-torsional coupled vibrations of a rotating shaft driven by a universal joint: Derivation of equations of motion and asymptotic analyses," *International Journal Series C-mechanical Systems Machine Elements and Manufacturing*, vol. 31, pp. 68-74, 1988.

[19] M. Kato, and H. Ota, "Lateral excitation of a rotating shaft driven by a universal joint with friction," ASME. *Journal of Vibration and Acoustics*, vol. 112, no. 3, pp. 298–303, 1990.

[20] H.A. DeSmidt, K.W. Wang, and E.C. Smith, "Coupled torsion-lateral stability of a shaft-disk system driven through a universal joint," ASME *Journal of Applied Mechanics*, vol. 69, no. 3, pp. 261–273, 2002.

[21] Y. Xia, J. Pang, C. Zhou, H. Li, and W. Li, "Study on the bending vibration of a Two-Piece propeller shaft for 4WD driveline," *SAE Technical Paper Series*, No. 2015-01-2174, 2015.

[22] Y. Xia, J. Pang, L. Yang, Z. Qin, and Y. Xianwu, "Nonlinear numerical and experimental study on the second-order torsional and lateral vibration of driveline system connected by cardan joint," *Journal of Vibration and Control*, vol. 26, no. 7–8, pp. 540–551, 2019.

[23] B.X. Tchomeni, A.A. Alugongo, and L. Masu, "Modeling and vibration analysis of twin-rotor system interconnected by a Hooke's joint (Part A). *Vibroengineering Procedia*, vol. 27, pp. 1–6, 2019.

[24] B.X. Tchomeni, and A.A. Alugongo, "Theoretical and experimental analysis of an unbalanced and cracked cardan shaft in the vicinity of the critical speed," *Mathematical Models in Engineering*, vol. 6, no. 1, pp. 34–49, 2020.

[25] M. Browne, and A. Palazzolo, "Super harmonic nonlinear lateral vibrations of a segmented driveline incorporating a tuned damper excited by non-constant velocity joints," *Journal of Sound and Vibration*, vol. 323, no. 1–2, pp. 334–351, 2009.

[26] M. SoltanRezaee, M.R. Ghazavi, and A. Nahafi, "Mathematical modelling for vibration evaluation of powertrain systems," *Proceedings of the IASTED International Conference on Modelling, Simulation and Identification, MSI 2017*, pp. 73-79, 2017.

[27] M. SoltanRezaee, M.R. Ghazavi, A. Najafi, and S. Rahmanian, "Stability of a multi-body driveshaft system excited through U-joints," *Meccanica*, vol. 53, no. 4–5, pp. 1167–1183, 2017.

[28] S.K. Bharti, and A.K. Samantaray, "Resonant capture and Sommerfeld effect due to torsional vibrations in a double Cardan joint driveline," *Communications in Nonlinear Science and Numerical Simulation*, vol. 97, p. 105728, 2021.

[29] W. Yao, and H. DeSmidt, "Nonlinear coupled Torsion/Lateral vibration and Sommerfeld behavior in a double U-Joint driveshaft," *Journal of Vibration and Acoustics*, vol. 143, no. 3, 2021.

[30] L. Murawski, and M. Dereszewski, "Theoretical and practical backgrounds of monitoring system of ship power transmission systems' torsional vibration," *Journal of Marine Science and Technology (Japan)*, vol. 25, pp. 272–284, 2020.

[31] M. Zajícek, and J. Dupal, "Analytic solution of simplified Cardan's shaft model," *Applied and Computational Mechanics*, vol. 8, 2014.

[32] A. Chaban, Z. Łukasik, A. Popenda, and A. Szafraniec, "Mathematical modelling of transient processes in an asynchronous drive with a long shaft including cardan joints," *Energies*, vol. 14, no. 18, p. 5692, 2021.

[33] G. Wu, W. Shi, and Z. Chen, "The effect of multi-universal coupling phase on torsional vibration of drive shaft and vibration of vehicle," *SAE Technical Paper*, No. 2013-01-1490, 2013.

[34] M. SoltanRezaee, M.R. Ghazavi, A. Najafi, and W. Liao, "Modeling and analysis of rotary mechanical systems linked through a U-joint," *International Journal of Mechanical Engineering and Robotics Research*, vol. 8, pp. 459–465, 2019.